Effects of Imperatoxin A on Local Sarcoplasmic Reticulum Ca^{2+} Release in Frog Skeletal Muscle

Alexander Shtifman,* Christopher W. Ward,* Jianli Wang,† Hector H. Valdivia,† and Martin F. Schneider*
*Department of Biochemistry and Molecular Biology, University of Maryland School of Medicine, Baltimore, Maryland 21201, and †Department of Physiology, University of Wisconsin School of Medicine, Madison, Wisconsin 53706 USA

ABSTRACT We have investigated the effects of imperatoxin A ($IpTx_a$) on local calcium release events in permeabilized frog skeletal muscle fibers, using laser scanning confocal microscopy in linescan mode. $IpTx_a$ induced the appearance of Ca^{2+} release events from the sarcoplasmic reticulum that are ~2 s and have a smaller amplitude (31 ± 2%) than the "Ca^{2+} sparks" normally seen in the absence of toxin. The frequency of occurrence of long-duration imperatoxin-induced Ca^{2+} release events increased in proportion to $IpTx_a$ concentrations ranging from 10 nM to 50 nM. The mean duration of imperatoxin-induced events in muscle fibers was independent of toxin concentration and agreed closely with the channel open time in experiments on isolated frog ryanodine receptors (RyRs) reconstituted in planar lipid bilayer, where $IpTx_a$ induced opening of single Ca^{2+} release channels to prolonged subconductance states. These results suggest involvement of a single molecule of $IpTx_a$ in the activation of a single Ca^{2+} release channel to produce a long-duration event. Assuming the ratio of full conductance to subconductance to be the same in the fibers as in bilayer, the amplitude of a spark relative to the long event indicates involvement of at most four RyR Ca^{2+} release channels in the production of short-duration Ca^{2+} sparks.

INTRODUCTION

According to currently accepted models, E-C coupling in skeletal muscle involves direct interaction between the voltage sensor in the T-tubule, the dihydropyridine receptor (DHPR), and the Ca^{2+} release channel of the sarcoplasmic reticulum (SR), the ryanodine receptor (RyR). Activation of the DHPR voltage sensor causes the opening of the RyR Ca^{2+} channel and subsequent Ca^{2+} release into the myoplasm, resulting in activation of the contractile apparatus (for a review see Meltzer et al., 1995; Schneider, 1994). Initial investigations provided evidence that the 138-amino acid cytoplasmic loop linking repeats II and III of the α_1 subunit of DHPR (II-III loop) is crucial for the E-C coupling in skeletal muscle (Tanabe et al., 1990). Experiments with isolated peptides from rabbit skeletal muscle have shown specific interactions between the Arg^{1076}-Asp^{1112} region of the RyR1 and the Thr^{671}-Leu^{690} region of the II-III loop (Leong and MacLennan, 1998). Other studies show that specific subsections of the II-III loop can induce Ca^{2+} release from the SR (El-Hayek et al., 1995) and partially restore skeletal-type E-C coupling in dysgenic myotubes (Nakai et al., 1998). These results provide strong evidence that the II-III loop is the primary activator of Ca^{2+} release in skeletal muscle; however, it is still undetermined which amino acid sequence interacts directly with the RyR. Furthermore, other segments of the II-III loop have been implicated in the modulation of the RyR activity (El-Hayek et al., 1995).

Imperatoxin A ($IpTx_a$) is a 33-amino acid peptide isolated form the venom of the scorpion *Pandinus imperator*. This peptide has three cysteine residues that stabilize its globular, three-dimensional (3D) structure by forming disulfide bridges (Zamudio et al., 1997). The primary structure of $IpTx_a$ resembles that of the Thr^{671}-Leu^{690} region of the II-III loop in that both peptides display a structural motif consisting of a cluster of basic residues followed by a hydroxylated amino acid (Ser or Thr) (Zamudio et al., 1997; Gurrola et al., 1999). Imperatoxin A interacts specifically and with high affinity with the skeletal and cardiac isoforms of RyR (Tripathy et al., 1998). Direct measurements of channel activity with RyR reconstituted in planar lipid bilayer demonstrate that addition of imperatoxin to the cytosolic side induces long-duration subconductance states. The substates are ~30% of full conductances, regardless of the current carrier species (Tripathy et al., 1998). $IpTx_a$ increases [^{3}H]ryanodine binding and enhances the activity of the Ca^{2+} release channels; both affects are modulated in a concentration-dependent manner (Gurrola et al., 1999). To test whether the II-III loop and $IpTx_a$ interact with the same modulatory site on RyR, competitive studies were conducted with both peptides. The results from these experiments demonstrate that the II-III loop displaces binding of $IpTx_a$ to the Ca^{2+} release channel and decreases its capacity to activate RyRs (Gurrola et al., 1999), thus suggesting an interaction with a defined amino acid sequence of the RyR. It thus appears that $IpTx_a$ provides an important tool for elucidating the E-C coupling mechanism.

Confocal imaging has become an important approach in monitoring Ca^{2+} release from the SR in functionally intact physiological systems (Cheng et al., 1993; Tsugorka et al., 1995; Klein et al., 1996; Lacampagne et al., 1996). The macroscopic [Ca^{2+}] transient appears to be a direct result of summation of individual Ca^{2+} release events induced by

Received for publication 25 February 2000 and in final form 11 May 2000.
Address reprint requests to Dr. Martin F. Schneider, Department of Biochemistry and Molecular Biology, University of Maryland School of Medicine, 108 N. Greene Street, Room 229, Baltimore, MD 21201. Tel.: 410-706-7812; Fax: 410-706-8297; E-mail: mschneid@umaryland.edu.

0006-3495/00/08/814/14 $2.00

depolarization of the fiber (Klein et al., 1997). Each discrete and localized elevation in myoplasmic [Ca^{2+}] (Ca^{2+} spark) is detected as a brief elevation of fluorescence of an indicator dye. In skeletal as well as cardiac muscle, individual Ca^{2+} sparks are believed to be released from a small cluster of SR Ca^{2+} release channels (Rios et al., 1999) or perhaps even a single channel (Schneider 1999). In skeletal muscle Ca^{2+} sparks have been shown to occur at low frequency without activation of the voltage sensor (Klein et al., 1996). These spontaneous Ca^{2+} release events can be activated by an increase in [Ca^{2+}] (Klein et al., 1996) or inhibited with increased [Mg^{2+}] (Lacampagne et al., 1998) in the myoplasm, which are both consistent with calcium-induced calcium release (Klein et al., 1996). The examination of individual Ca^{2+} release event properties provides an important means of elucidating the mechanism underlying Ca^{2+} release during the process of E-C coupling.

In the present study we have investigated the effect of $IpTx_a$ on localized Ca^{2+} release events in permeabilized frog skeletal muscle fibers and characterized the differences between spontaneous Ca^{2+} sparks and imperatoxin-induced Ca^{2+} release events. We found that $IpTx_a$ induces long-duration, low-amplitude Ca^{2+} release events without altering the properties of Ca^{2+} sparks. The frequency of the long-duration events is concentration dependent, in a manner suggesting the involvement of a single Ca^{2+} release channel in the generation of an individual $IpTx_a$-induced long-duration Ca^{2+} release event. Some of these results have been presented in abstract form (Shtifman et al., 1999).

MATERIALS AND METHODS

Preparation of skeletal muscle fibers

Experiments were performed on cut segments of single fibers isolated from ileofibularis muscle of frogs (*Rana pipiens*). Frogs were killed by decapitation and subsequent spinal cord destruction. Removed muscle was pinned in a dissecting chamber containing Ringer's solution. Single fiber segments (3–5 mm) were manually dissected in the relaxing solution containing (in mM) 120 K-glutamate, 2 $MgCl_2$, 0.1 EGTA, 5 Na-Tris-maleate (pH 7.00). Cut fiber segments were mounted under stretch in a custom chamber as described by Lacampagne et al. (1998). The chemical permeabilization was realized by exposing the fiber to the relaxing solution containing 0.005% saponin for 45 s. The solution in the chamber was then changed to an internal solution containing (in mM) 80 Cs-glutamate, 20 creatine phosphate, 4.5 Na-Tris-maleate, 13.2 Cs-Tris-maleate, 5 glucose, 0.1 EGTA, 1 dithiothreitol, 0.05 Fluo-3 (pentapotassium salt) (Molecular Probes, Eugene, OR), 5.50 or 6.73 $MgCl_2$ (0.65 or 1.2 $Mg^{2+}{}_{free}$), and 5 Na-ATP. The estimated $[Ca^{2+}]_{free}$ was 0.1 μM. To avoid the osmotic effects of chemical permeabilization, 8% dextran was added to the solution (Tsuchiya, 1988; Ward et al., 1998).

Fluorescence measurements

Ca^{2+} release events were measured using a laser scanning confocal system (MRC 600; Bio-Rad Laboratories, Hercules, CA) interfaced with an inverted microscope (IX-70, with a 60×, 1.4 NA oil immersion objective; Olympus Corp., Lake Success, NY). All experiments were conducted at room temperature (22°C). Measurements were obtained in linescan mode (x versus t) at a sampling rate of 500 Hz (2 ms/line), with the scan line oriented parallel to the muscle fiber. The pixel size was 0.18 μm in x and 2 ms in t, and the image dimensions were 138 μm for x and 1024 ms for t. For maximum resolution images were acquired very close to the bottom surface of the fiber. Each run consisted of five images, with each successive image separated from the last by a 1-s gap, acquired at the same location. To avoid laser damage, the scan line was moved 0.9 μm perpendicular to the long axis of the fiber after each run.

Initial recordings were obtained while the fibers were bathed in an internal solution (control). Subsequent to this, fibers were bathed in an internal solution containing the appropriate concentration of $IpTx_a$.

Analysis of linescan images

Linescan images were first computer processed to automatically identify and store spark locations, using a relative threshold algorithm as described by Cheng et al. (1999). This algorithm was successful at identifying the location of short-duration Ca^{2+} sparks; however, long-duration Ca^{2+} release events were occasionally misidentified and were subsequently manually identified. After the autodetection algorithm, linescan images were converted to images of change in fluorescence (ΔF) by subtracting the average fluorescence (F) of the five sequential images, excluding the fluorescence at the identified Ca^{2+} spark locations, at each spatial location from each raw fluorescence image. Each ΔF image was then divided by F to create a $\Delta F/F$ image.

Discrete "short-duration" Ca^{2+} sparks were analyzed as previously described by our laboratory (Lacampagne et al., 1998). In brief, images were smoothed to reduce noise (3 × 3 pixel "boxcar" routine), and identified Ca^{2+} spark locations were redisplayed in $\Delta F/F$. Plots of the temporal (t) profiles at the spatial center of the spark were constructed by averaging five pixels (0.9 μm) in x (centered at the x location of the peak value for $\Delta F/F$). Plots of spatial (x) distribution of fluorescence at the time of the peak were constructed by averaging three pixels (6 ms) in t (centered at the t location of the peak value of $\Delta F/F$). Both plots were then expanded 10 times (linear interpolation) to increase the apparent resolution. Sparks were selected based on the following criteria: a change in $\Delta F/F \geq 0.3$, full-duration at half-maximum amplitude (FDHM) $\geq$ 6ms, and full-width at half-maximum amplitude (FWHM) ≥ 1 μm. The rise time of the events was taken as the time from 10% to 90% of the maximum amplitude. The peak $\Delta F/F$ was determined by the maximum value in the temporal profile.

Long-duration Ca^{2+} release events were displayed in $\Delta F/F$ images as described above. For each identified event, a temporal time course (t) was constructed by averaging five pixels (0.9 μm) centered at the spatial peak ΔF/F of the entire event (determined by a Gaussian fit). The temporal plot was used to visually identify the start and end time, and the duration was then determined. The mean FWHM of the event was determined from the longest contiguous portion of the fluorescence transient, which was uninterrupted by a short-duration Ca^{2+} spark. Furthermore, spatial width was calculated at 10-ms intervals (average of five temporal pixels; 10 ms) from the beginning of the event. Long-duration Ca^{2+} release events were selected based on the following criteria: amplitude ≥ 0.15 $\Delta F/F$, duration $\geq$ 100 ms. Any short-duration Ca^{2+} sparks superimposed on the long-duration event were analyzed as described previously. Results are expressed as mean ± SEM.

Single-channel recordings in planar lipid bilayers

Reconstitution of frog skeletal muscle SR vesicles into planar lipid bilayers for single-channel recordings of RyRs was carried out as described for canine cardiac SR at 22°C (Valdivia et al., 1995). Briefly, a bilayer of phosphatidylethanolamine:phosphatidylserine (1:1 dissolved in n-decane to 25 mg/ml) was "painted" with a glass rod across an aperture of ~250 μm diameter in a delrin cup. The *cis* chamber was the voltage control side connected to the headstage of a 200-A Axopatch amplifier, and the *trans*

side was held at virtual ground. The *cis* (500 μl) and *trans* (600 μl) chambers were initially filled with 50 mM cesium methanesulfonate and 10 mM Na-HEPES (pH 7.2). After bilayer formation, an asymmetrical cesium methanesulfonate gradient (300 mM *cis*/50 mM *trans*) was established, and the SR vesicles were then added to the *cis* chamber, which corresponded to the cytoplasmic side of the SR, and the *trans* side corresponded to the lumenal side. Contaminant Ca^{2+} (3–5 μM) was sufficient to elicit channel activity. After the detection of channel openings, Cs^+ in the *trans* chamber was raised to 300 mM to dissipate the chemical gradient and prevent further vesicle fusion. For each condition, single-channel data were collected at steady voltages (+30 and −30 mV) for 2–4 min. For recording of Ca^{2+} currents through Ca^{2+} release channels, an asymmetrical gradient of (*cis*/*trans*) 200/100 mM Cs^+-methanesulfonate in the presence of 10 mM $CaCl_2$ in the *trans* (lumenal) side of the channel was used for channel fusion. After the detection of channel openings, recordings were made at −17 mV, the reversal potential (E_{rev}) for Cs^+. In this configuration, channel openings, corresponding mostly to Ca^{2+} currents, appeared as downward deflections of the baseline current but have been inverted in Fig. 3 to facilitate comparison with Cs^+ currents and fluorescence records. Signals were analyzed after filtering with an eight-pole low-pass Bessel filter at a sampling frequency of 1.5–2 kHz. Data acquisition and analysis were done with Axon Instruments (Burlingame, CA) software and hardware (pClamp v6.0.3, Digidata 1200 AD/DA interface). The probability of an $IpTx_a$-induced substate occurrence ($P_{substate}$), defined as the time spent in the subconductance state, divided by total recorded time, was obtained by constructing all-points amplitude histograms and fitting the data with Gaussian functions (Tripathy et al., 1998).

RESULTS

Induction of long-duration Ca^{2+} release events by $IpTx_a$ in frog skeletal muscle fibers

Fig. 1 presents the effects of $IpTx_a$ on linescan images from permeabilized frog muscle fibers. Three consecutive linescan fluorescence ($\Delta F/F$) images of the control (Fig. 1 *A*) and three consecutive images after the addition of imperatoxin (Fig. 1 *B*) are shown in Fig. 1. In each image, the distance along the fiber (x) is represented vertically and the time (t) is represented horizontally to give an x versus t in each image.

Fig. 1 *A* shows a representative series of images in the control condition in which fibers were bathed in internal solution with 0.65 mM $[Mg^{2+}]_{free}$ and Ca^{2+} indicator. Each localized increase in $[Ca^{2+}]$, a Ca^{2+} spark, is characterized by a brief and localized increase in fluorescence (Klein et al., 1996; Schneider and Klein, 1996). The $\Delta F/F$ time courses at individual triads exhibiting activity are marked by arrowheads at the left and displayed below each linescan image. For each event, the amplitude ($\Delta F/F$), the temporal rise time (time required for fluorescence to rise from 10% to 90% of maximum amplitude), the spatial half-width (FWHM), and the half-duration (FDHM) were determined. The mean values for these parameters are as follows: amplitude, 0.63 ± 0.02 $\Delta F/F$; rise time, 5.98 ± 0.07 ms; FWHM, 2.04 ± 0.04 μm; FDHM, 13.3 ± 0.2 ms ($n_{fibers} = 5$).

Fig. 1 *B* demonstrates the effects of $IpTx_a$ on local Ca^{2+} release events. Here the fiber was incubated in the same internal solution as the control with the addition of 5 nM $IpTx_a$ for 15 min before the start of image acquisition. In addition to the spark type release seen in Fig. 1 *A*, the addition of $IpTx_a$ induces the appearance of long-duration Ca^{2+} release events (>100 ms), as indicated by prolonged local increase in fluorescence in the linescan images in Fig. 1 *B* (*top, arrows*) and the long duration of elevated fluorescence at the three monitored triads in Fig. 1 *B* (*bottom*). The experimental conditions allowed for the frequency of Ca^{2+} sparks to remain relatively similar in the control (0.17 ± 0.027 $sarc^{-1}{\cdot}s^{-1}$) and $IpTx_a$ conditions (0.2 ± 0.043 $sarc^{-1}{\cdot}s^{-1}$). The frequency of long events in the presence of $IpTx_a$ was 0.0039 ± 0.001 $sarc^{-1}{\cdot}s^{-1}$. Further analysis of the standard, short-duration Ca^{2+} sparks, after exposure to $IpTx_a$, has demonstrated that the mean spark parameters, such as the amplitude (0.55 ± 0.06 $\Delta F/F$), rise time (5.7 ± 0.04 ms), half-width (1.94 ± 0.08 μm), and half-duration (12.89 ± 0.6 ms), as well as the distribution of these parameters, remained virtually identical in controls and over a range of $[IpTx_a]$. This leads us to believe that the qualitatively different long-duration events that are not normally seen in the control condition are attributed to the $IpTx_a$-induced Ca^{2+} release events.

Fig. 2 presents sets of $\Delta F/F$ time courses of several $IpTx_a$-induced events at individual triads in different fibers. It is clearly shown that the duration of these long events greatly exceeds the duration of a regular, non-toxin-induced "short" spark. In Fig. 2 *A*, some of the events have a spark-like beginning, shown by the rapid increase in fluorescence amplitude, followed by a decrease and subsequent attainment of constant amplitude. There are also long events that do not begin with a spark; these events reach the amplitude plateau without the fluorescence spike at the beginning. In the fibers in the series of experiments for Figs. 1 and 2, 38% of long events began with a spark. Moreover, some of the imperatoxin-induced events appear to have a spark-like spike in fluorescence superimposed on the steady phase of the long event. As shown in Figs. 1 and 2, the long-duration $IpTx_a$-induced events have amplitudes smaller than the peak amplitude of the short-duration Ca^{2+} sparks.

A difficulty with the detection and characterization of the long sparks is that their duration is often longer then 1 s. Therefore, within a given 1-s linescan image, most of the events are detected as a change in fluorescence either at the beginning or at the end of their time course. Fig. 2 *A* shows representative $\Delta F/F$ time courses of the events that were detected at the start of their time course, and Fig. 2 *B* shows events selected at the end of the time course. The long duration and steady-state amplitude of the $IpTx_a$-induced events can be explained by the prolonged binding of the toxin to the channel, which would allow the release of Ca^{2+} from the channel to reach a steady state with the processes of Ca^{2+} diffusion and Ca^{2+} binding to regulatory proteins of the contractile apparatus and other Ca^{2+} binding sites. It is unlikely that channels not bound by toxin could contrib-

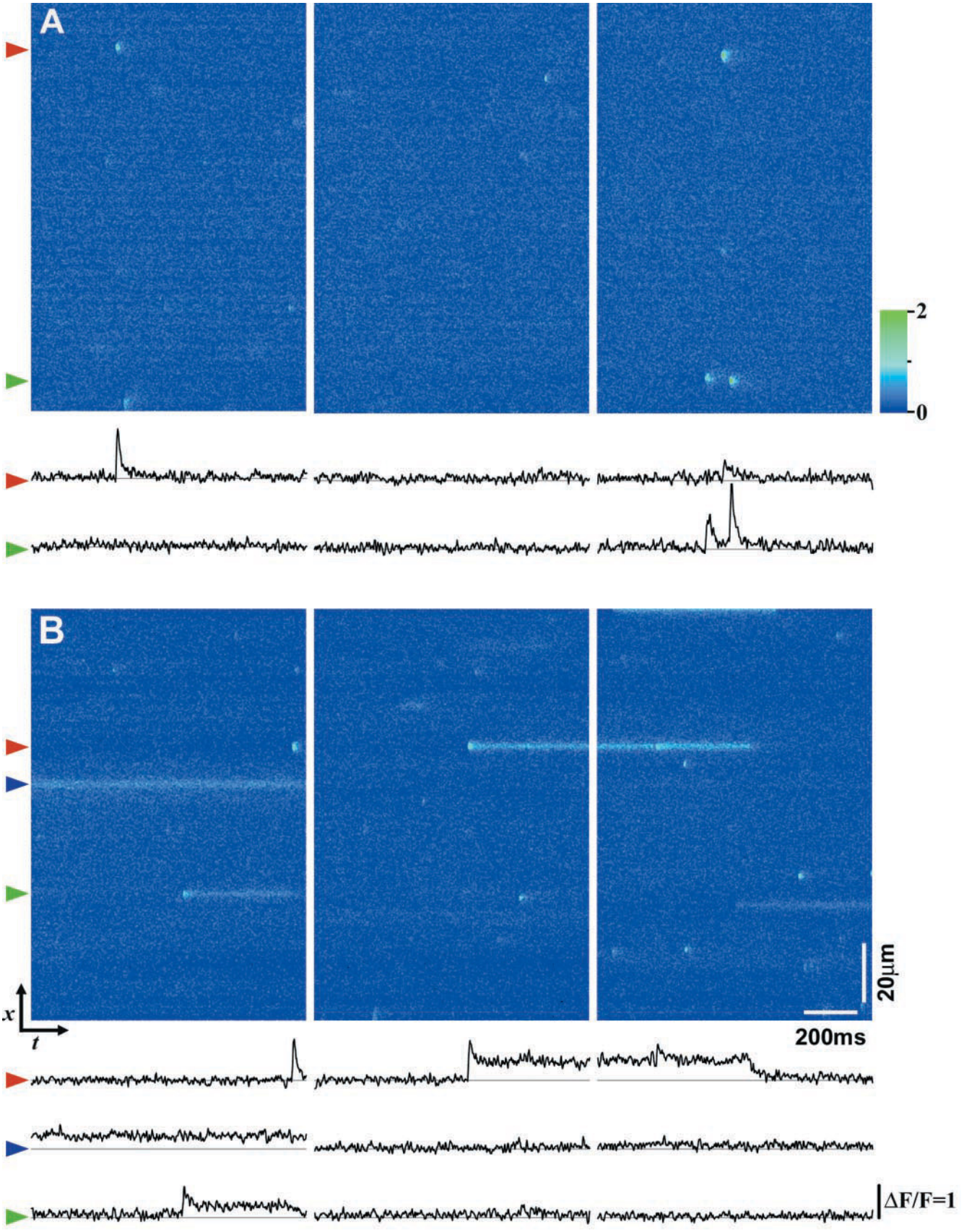
A
2
0
B
20μm
200ms
x
t
ΔF/F=1

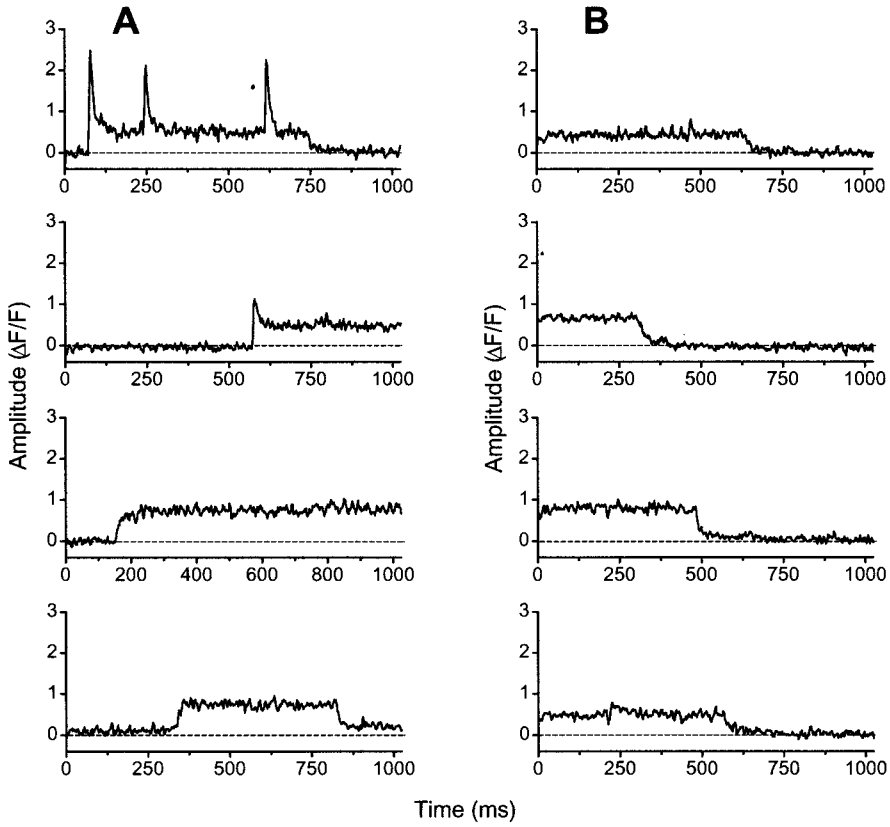

FIGURE 2 Representative time courses of $IpTx_a$-induced Ca^{2+} release events in permeabilized muscle fibers. (*A*) $\Delta F/F$ time courses at eight individual triads from different fibers showing $IpTx_a$-induced events with a detectable beginning of fluorescence time course, (*B*) as well as the events with only detectable end of fluorescence time course.

ute to the long-duration $IpTx_a$-induced events. Any toxin free channels activated by Ca^{2+}-induced Ca^{2+} release (CICR) due to locally elevated $[Ca^{2+}]$ near an open $IpTx_a$-bound channel would be expected to rapidly inactivate. Such inactivated channels would then be unable to contribute to a prolonged event.

The long-duration Ca^{2+} release events in Figs. 1 and 2 were obtained from sets of five 1-s duration linescan images recorded with ~1-s separations between successive images. If the long events observed here represent randomly occurring events with time-independent properties, then the mean frequency of occurrence of events as well as the total uration of events per second of recording should both be independent of whether the parameters were determined during a single prolonged period of continuous recording or during a series of recordings separated in time. Thus the values of these parameters obtained from our series of 1-s linescan images should represent accurate estimates of the respective parameters. Consequently, these parameters can be used to estimate the mean duration of a toxin-induced event, which is given by the ratio of the total event duration per second of recording divided by the frequency of occurrence of the long events. The average value of the mean event duration calculated in this way for the five fibers in the series of experiments illustrated in Figs. 1 and 2 was 2.6 ± 0.6 s. This value is considerably greater than 1 s and thus is clearly consistent with the observation that a large fraction of the detected events extend before or after or even throughout a single 1-s duration linescan image (Figs. 1 and 2).

Induction of subconductance states by $IpTx_a$ in single channels isolated from frog SR

Fig. 3 demonstrates that the addition of $IpTx_a$ to the cytoplasmic (*cis*) side of frog skeletal RyR reconstituted in planar lipid bilayer induces the appearance of long-duration subconductance states. The mean percentage ratio of the subconductance current relative to the current of the full

FIGURE 1 Effects of $IpTx_a$ on SR Ca^{2+} release in frog skeletal muscle. (*Top*) Consecutive fluorescence line scan images and (*bottom*) time courses of $\Delta F/F$ at the indicated individual triads, under control (*A*) and $IpTx_a$ (*B*) conditions. The individual triad $\Delta F/F$ time courses correspond to the average of five pixels in *x* at the location (*arrowhead*) of identified triads. The acquisition was started during exposure of the fiber to an internal solution containing a $[Mg^{2+}]_{free}$ of 0.65 mM (control). The solution was then changed for an internal solution containing an additional $[IpTx_a]$ of 5 nM. Fibers were incubated for 15 min in the presence of imperatoxin before the start of image acquisition.

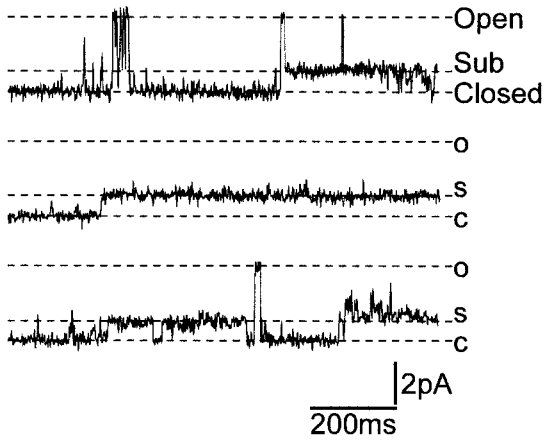

FIGURE 3 Functional effects of $IpTx_a$ on skeletal RyRs. Single Ca^{2+} release channel recordings with Ca^{2+} as the current carrier. Frog SR vesicles were reconstituted in lipid bilayers in (*cis/trans*) 200/100 mM Cs^+-methanesulfonate and 10 mM $CaCl_2$ in the *trans* (lumenal) side. Traces were obtained at a holding potential of −17 mV, ~1 min after the addition of 100 nM $IpTx_a$ to the *cis* (cytoplasmic) side.

conductance state was 27.8 ± 3% ($n_{channels}$ = 4) for Ca^{2+} conductance in frog SR Ca^{2+} release channel reconstituted in planar lipid bilayer. The Ca^{2+} currents presented here show that $IpTx_a$-induced events display lower amplitudes and a mean open time more than 100-fold longer than that of unmodified channels. Fig. 3 also shows that a fraction of $IpTx_a$-modified channels open to a brief, full conductance state, which is followed by a prolonged subconductance state, whereas other channels achieve a subconductance state immediately. In some cases Ca^{2+} currents also appear to alternate between prolonged subconductance and brief openings to a full conductance state. These observations are analogous to the Ca^{2+} release event time courses in Fig. 2, where two modes of initiation of long-duration Ca^{2+} release events as well as the sparks superimposed on the steady phase of the events are observed in permeabilized muscle fibers.

Concentration dependence of $IpTx_a$ effects on muscle fibers

Because an individual frog Ca^{2+} release channel in a bilayer is capable of generating long-duration, low-amplitude currents in the presence of $IpTx_a$, it is likely that the long-duration Ca^{2+} release events observed in the permeabilized frog muscle fibers in the presence of imperatoxin are also generated by the opening of a single Ca^{2+} release channel. To test this hypothesis, we examined the concentration dependence of $IpTx_a$ effects on muscle fibers to see if they were consistent with the binding of a single imperatoxin molecule to produce a long-duration event.

Fig. 4 demonstrates that $IpTx_a$ elicited long-duration Ca^{2+} release events in frog muscle fibers in a dose-dependent manner. In these experiments the initial set of control images was acquired while the fibers were bathed in an $IpTx_a$-free internal solution with 1.2 mM $[Mg^{2+}]_{free}$ (see Materials and Methods). This solution was exchanged for the same internal solution containing 10, 25, or 50 nM added $IpTx_a$. Fibers were incubated in toxin-containing solution for 15 min before the start of image acquisition. To provide a common reference condition for each fiber, the same fibers were later incubated in internal solution containing 50 nM $IpTx_a$ for an additional 15 min before a final period of image acquisition. Images in each condition were acquired at different positions along the fiber to avoid laser damage. Fig. 4 *A* shows that the frequency of occurrence of toxin-induced long-duration events increased approximately in direct proportion to $[IpTx_a]$. Thus the initiation of the long events by toxin appears to follow a first-order response, suggesting the interaction of a single molecule of $IpTx_a$ with a single RyR to produce the activation of a prolonged, sublevel of Ca^{2+} release.

Fig. 4 *B* shows the effect of $[IpTx_a]$ on the total duration of long Ca^{2+} release events. In this figure, the total duration of all detectable toxin-induced events per second of recording is presented. Thus, in contrast to the event frequencies presented in Fig. 4 *A*, which include only toxin-induced events in which the start of the event was captured in a recorded linescan image, Fig. 4 *B* includes all long events that begin or end within an image, as well as those that continue throughout a 1-s image. Fig. 4 *B* shows that the total duration of the long, toxin-induced Ca^{2+} release events was also proportional to the concentration of imperatoxin.

Fig. 4 *C* shows the $[IpTx_a]$ dependence of the mean duration of a toxin-induced event, which is given by the ratio of the total event duration per second of recording in a fiber, divided by the frequency of occurrence of the long events in the same images from the fiber. This ratio is essentially independent of $[IpTx_a]$, indicating that the mean duration of an individual toxin-induced event was the same at all toxin concentrations. Because only the off-rate influences the channel open time, the present observation of constant toxin-induced event duration at all $[IpTx_a]$ is consistent with the results of previous single-channel experiments, where the off-rate of $IpTx_a$ from the channel was independent of the $[IpTx_a]$ and only the on-rate was dependent on concentration of this ligand (Tripathy et al., 1998). Thus the increase in total duration of toxin-induced events observed here with increasing $[IpTx_a]$ was due exclusively to an increase in the frequency of occurrence of toxin-induced events, with no change in the mean duration of the events that occur at any toxin concentration. The calculated mean duration of the long events at all toxin concentrations tested in the fibers in this series of experiments was ~1.8 s, again consistent with the observation that a large fraction of the detected events extend before or after a single 1-s duration linescan image.

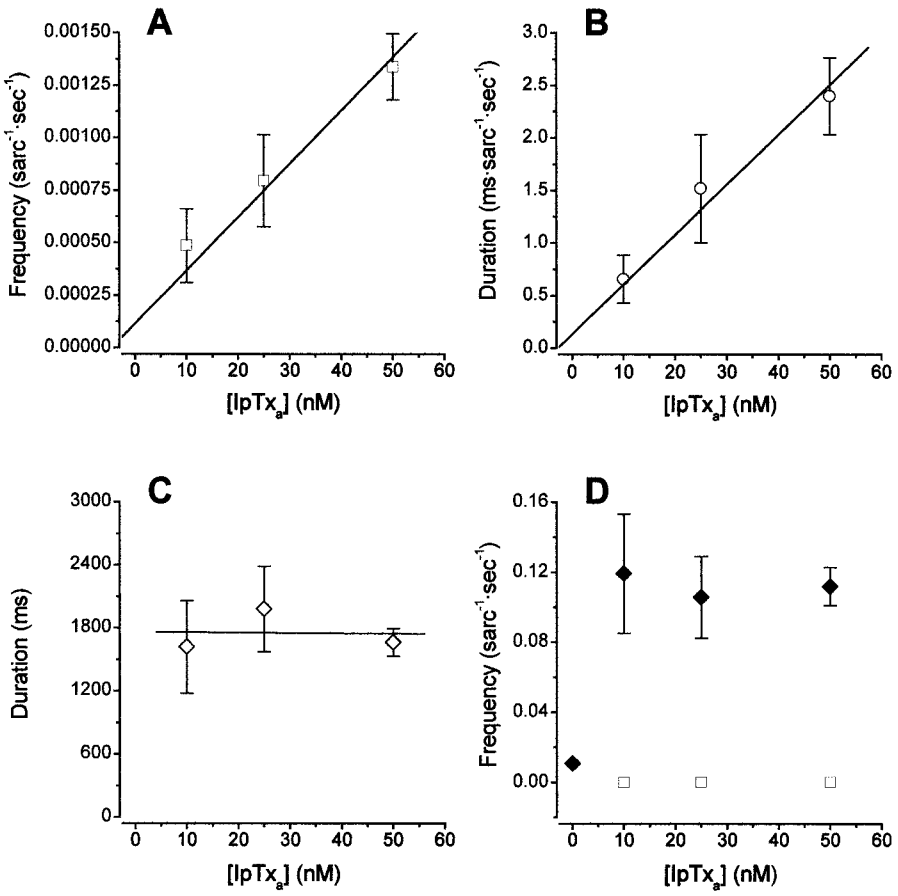

FIGURE 4 Concentration dependence of $IpTx_a$ effects on muscle fibers. (*A*) Frequency of induction of long-duration Ca^{2+} release events by $IpTx_a$ (□) at 10 nM (n_{fibers} = 6), 25 nM (n_{fibers} = 7), and 50 nM [$IpTx_a$] (n_{fibers} = 13). (*B*) Total duration of $IpTx_a$-induced events, plotted as a function of [$IpTx_a$] (○). (*C*) Mean duration of $IpTx_a$-induced events (◇). (*D*) Comparison of frequency between $IpTx_a$ -induced events (□) and Ca^{2+} sparks (◆) detected in the same linescan images at [$IpTx_a$] of 10, 25, and 50 nM, as well as under control conditions ([$IpTx_a$] 0 nM).

Fig. 4 *D* demonstrates that at all $IpTx_a$ concentrations used in muscle fibers, the frequency of occurrence of long-duration toxin-induced events (*open squares*) was very small compared with the frequency of occurrence of short-duration Ca^{2+} sparks (*filled diamonds*). Even at 50 nM IpTxa, the highest concentration used in these muscle fiber studies, the mean frequency of occurrence of imperatoxin-induced events (0.0013 ± 0.0002 $sarc^{-1}{\cdot}s^{-1}$) was ~100-fold lower than the mean frequency of short-duration Ca^{2+} sparks (0.11 ± 0.01 $sarc^{-1}{\cdot}s^{-1}$) recorded in the same linescan images. The relatively low frequency of the long events indicates that even at the highest tested [$IpTx_a$], only a small fraction of channels were modulated by the imperatoxin, and that the [$IpTx_a$] was thus probably far from possible dose-dependent saturation. However, the present experimental approach did not allow for testing [$IpTx_a$] much greater then 50 nM in muscle fibers. At concentrations greater than 50 nM, imperatoxin began to induce a general Ca^{2+} release from the SR, which caused an increase in baseline fluorescence that rendered the smaller amplitude events indistinguishable from the background noise. Fig. 4 *D* also shows that the spark frequency in the toxin condition, although higher than that in the controls in this series of experiments, remained essentially constant over the range of [$IpTx_a$]. Thus the dose dependence of the long-duration events was not influenced by any [$IpTx_a$]-dependent difference in Ca^{2+} spark frequency. The reason for the difference in Ca^{2+} spark frequency between the control and $IpTx_a$-containing conditions is currently undetermined.

As demonstrated in Fig. 2, a fraction of imperatoxin-induced Ca^{2+} release events originate with a spark, whereas other $IpTx_a$-induced long events do not appear to begin with a spark. The long events with a spark at the origin constituted 30% of all imperatoxin-induced long-duration Ca^{2+} release events in the fibers for the experiments in Fig. 4.

Concentration dependence of $IpTx_a$ effects on single Ca^{2+} release channels in bilayers

The concentration dependence of the effects of $IpTx_a$ was also investigated using frog SR vesicles incorporated into lipid bilayers. In these experiments Cs^+ was used as the current carrier to increase the channel current and thus improve the detection of channel opening (Fig. 5). Over the [$IpTx_a$] range from 10 to 100 nM, which spans the concentrations (10 to 50 nM) used to study the concentration dependence of long-duration toxin-induced events in frog muscle fibers, increasing the $IpTx_a$ concentration caused a concentration-dependent increase in the probability of the

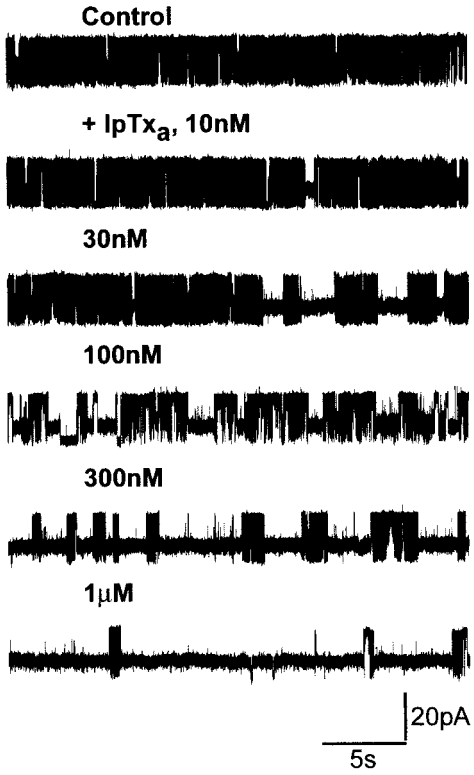

FIGURE 5 Dose response of the $IpTx_a$ effect on a frog skeletal Ca^{2+} release channel. Single-channel traces in the absence (control) and the presence of the indicated concentrations of $IpTx_a$ in the *cis* (cytoplasmic) side of the channel. Recording conditions were the same as those described in the legend to Fig. 3 and under Materials and Methods. Note different time scale.

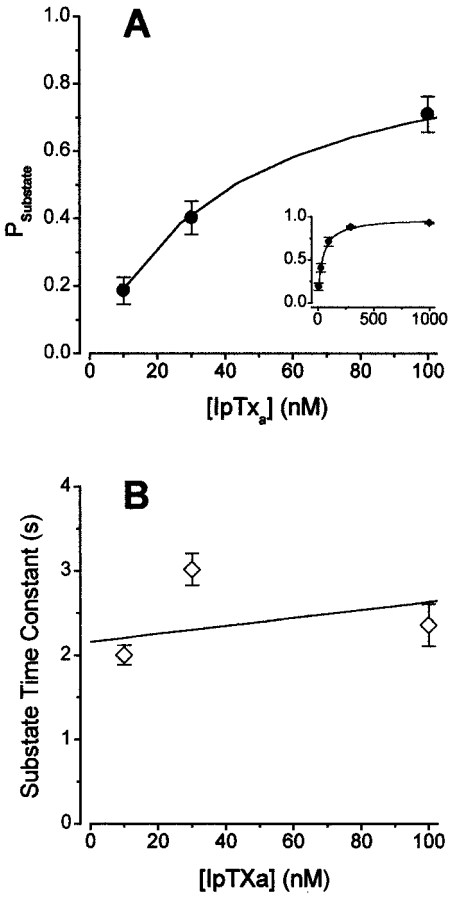

FIGURE 6 (*A*) Probability of occurrence of imperatoxin-induced subconductance state as a function of $[IpTx_a]$ determined from single-channel recordings described in Fig. 6. (*B*) Substate time constant at $[IpTx_a]$ of 10, 30, and 100 nM.

subconductance state for channels in the bilayer (Figs. 5 and 6 *A*). Using concentrations of $IpTx_a$ up to 1 μM, we found the full concentration dependence of the probability of the subconductance state to follow the concentration dependence for a single binding site with an apparent dissociation constant of 41nM and a maximum substate probability of 0.98 (Fig. 6 *A, inset*).

Despite the marked increase in $P_{substate}$ as $[IpTx_a]$ was increased from 10 to 100 nM in the bilayer studies (Fig. 6 *A*), the substate time constant was independent of $[IpTx_a]$ (Fig. 6 *B*). The time constant of the substate is equal to the mean duration of the $IpTx_a$-induced subconductance openings of the channel (Colquhoun and Hawkes, 1983). Thus the mean time constant of 2.5 s, determined from exponential fits of the open times of the long-duration subconductance openings measured at 10, 30, and 100 nM $IpTx_a$, using frog SR Ca^{2+} release channels in bilayers (Fig. 6 *B*), agrees very well with the mean durations of the long events measured in frog permeabilized muscle fibers at 10, 25, and 50 nM $IpTx_a$ (1.78 $\pm$ 0.125 s) (Fig. 4 *C*) and the mean duration of long events (2.6 $\pm$ 0.6 s) measured in experiments described in Fig. 2. Thus the duration of the toxin-induced long-duration open state appears to be quite similar in bilayers and in muscle fibers, indicating a similarity of imperatoxin-induced channel gating in the two experimental conditions. These observations provide further support for the idea that the duration of opening of a single SR Ca^{2+} release channel may determine the duration of the toxin-induced long release events monitored in muscle fibers.

Ca^{2+} release channel activity levels in the muscle fiber and bilayer experiments

The probability that a single SR Ca^{2+} release channel was active was vastly different in the bilayer and muscle fiber experiments presented here. In the bilayer, only a single channel was studied, so that channel had to exhibit a relatively high rate of activity for us to be able to obtain meaningful data in a practical amount of recording time. In contrast, in the muscle fiber there were ~50–100 Ca^{2+} release channels located within the ~1-μm-diameter confocal volume sampled at each triad (Franzini-Armstrong et al., 1999), and the linescan included ~40–50 triads. Thus in the muscle fiber studies the experimental conditions had to

be adjusted to give extremely low rates of activity in each channel, so that the activity of an individual toxin-modified channel could be distinguished from the activity of other channels at the same triad.

The differences in individual channel activity levels in the bilayer and muscle fiber studies can be quantitated using the data presented here. In the muscle fiber experiments, the total duration of toxin-induced long events at the highest concentration of $IpTx_a$ (50 nM) was only 2.4 ± 0.4 ms·sarc^{-1}·s^{-1} (Fig. 4 *B*), which corresponds to a fractional event time of 2.4×10^{-3} at each triad. If there were only a single Ca^{2+} release channel located at each triad this value would equal the open probability of that channel. However, because there may be ~50–100 Ca^{2+} release channels located within the confocal volume sampled at each triad (Franzini-Armstrong et al., 1999), if each long event corresponds to the opening of a single channel, then the channel open probability would have been 50–100 times lower, or only $2.4–4.8 \times 10^{-5}$. Thus for the conditions in these muscle fiber experiments the toxin occupancy of channels was vanishingly small. In contrast, in the bilayer experiments the probability of the toxin-induced substate was ~0.5 for a toxin concentration of 50 nM (Fig. 6 *A*). This is at least 200 times larger, and possibly as much as 10,000–20,000 times larger, than the probability of occurrence of the long-duration toxin-induced channel openings in the muscle fiber experiments at the same concentration of $IpTx_a$. Thus the toxin had a much higher apparent affinity for the channels in the bilayer experiments than in the muscle fiber experiments.

Because the toxin interacts with the open channel (Tripathy et al., 1998), the higher apparent affinity of the toxin for the channel in the bilayer experiments may have been due to the higher probability that a channel was open to the full-conductance state in the bilayer experiments than in the muscle fiber studies. The probability of the SR Ca^{2+} release channels being in the full-conductance open state was directly determined to be 0.22–0.88 in the bilayer experiments before toxin addition. In the muscle fiber experiments in Fig. 4 *D* the frequency of brief Ca^{2+} sparks was ~0.12 sarc^{-1}·s^{-1} in the presence of toxin. If the mean open time of the channel(s) generating the spark was ~5 ms (Lacampagne et al., 1999), then the open probability would have been less than 6.0×10^{-4} if all channels at a triad contribute to the generation of a spark. However, if only a fraction of the channels at each triad contribute to the spark, then the open probability of each channel would be correspondingly smaller. Thus the probability of being in the full-conductance open state was at least ~400–1400 times higher in the bilayer than in the muscle fiber experiments and even larger if only a fraction of the channels at triad participate in each spark. This large difference in the probability of occurrence of the normal, full-conductance open state in fibers and bilayer largely accounts for the great difference in probability of the toxin-induced subconductance state in the bilayer and muscle fiber experiments, because the toxin appears to interact with the full open channel to induce the long-duration subconductance state (Tripathy et al., 1998).

Spatiotemporal properties of $IpTx_a$-induced events in permeabilized fibers

Analysis of the properties of sparks that occur at the beginning of the imperatoxin-induced events has shown that these sparks do not differ from non-toxin-induced sparks in their amplitude (0.83 ± 0.05 $\Delta F/F$), rise time (5.4 ± 0.17 ms), or half-width (1.87 ± 0.05 μm). This allowed for the accurate comparison of Ca^{2+} spark properties, namely the amplitude and spatial half-width, with the properties of the long events at their steady state, using events that presumably occur at the same spatial location. The mean value of the ratio of steady fluorescence to peak spark fluorescence in the same events was 31 ± 0.2%. Fig. 7 *A* presents mean values of the average amplitude of the steady region of the long events, the peak amplitude of the spark at the beginning of the same long events, and the average peak amplitude of sparks not associated with long events. Fig. 7 *B* demonstrates the differences in spatial half-widths of the same events described in Fig. 7 *A*. At steady state the spatial half-widths are greater for the long-duration toxin-induced events compared to the sparks. The increase in half-width may be due to the prolonged and increased total release in Ca^{2+} produced by the prolonged presence of the imperatoxin A in the channel.

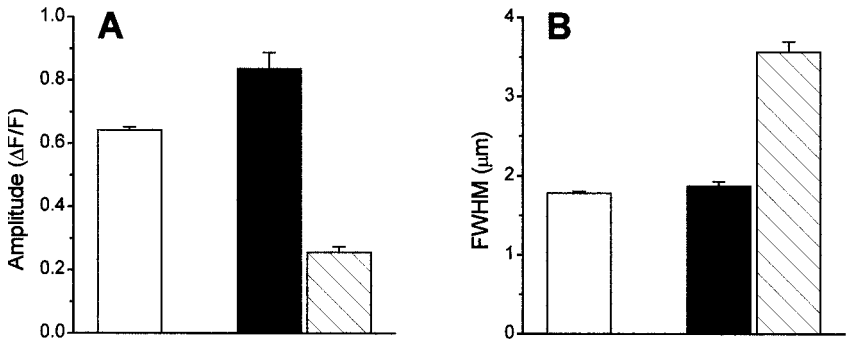

FIGURE 7 Spatiotemporal properties of $IpTx_a$-induced events from all tested conditions in Fig. 4. (*A*) Comparison of average Ca^{2+} spark amplitude (□) (n_{events} = 27,236) with an average amplitude of a spark in the beginning of imperatoxin-induced events (■) (n_{events} = 62) and the amplitude of the steady region of the long Ca^{2+} release events (▨) (n_{events} = 62). (*B*) Comparison of spatial half-widths of the events in *A*.

Spatiotemporal properties of averaged imperatoxin-induced events are shown in Fig. 8. Fig. 8, *A* and *B*, demonstrates the differences in the time courses of long events that have a spark-like beginning versus the events that do not. As expected (Fig. 7), events in Fig. 8 *A* originate with a spike in fluorescence with a mean amplitude of ~0.8 units of $\Delta F/F$ that is followed by a rapid decay and attainment of the steady state with a mean amplitude of ~0.2 $\Delta F/F$. Events that do not originate with a spark at the beginning of their time course achieve the steady state much more rapidly (<5 ms) and appear to have a mean fluorescence amplitude of ~0.2 $\Delta F/F$. Fig. 8, *C* and *D*, compares the spatial half-widths of long events averaged in Fig. 8, *A* and *B*, respectively. It is apparent that the events that begin with a spark have a smaller half-width at the beginning of their time course and achieve the peak mean half-width of ~4 μm within the first 10 ms. Events that do not begin with a spark appear to originate with a larger half-width but have a mean half-width similar to that of the above-described events.

DISCUSSION

This article describes $IpTx_a$-induced, discrete long-duration, low-amplitude Ca^{2+} release events in skeletal muscle fibers, as detected by laser scanning confocal microscopy. Our results demonstrate that $IpTx_a$ modulates SR Ca^{2+} release channels in permeabilized fibers without altering the properties of individual, short-duration Ca^{2+} sparks. It is important to note that the data presented here were obtained under conditions where the structural environment of the triad junction and its accessory proteins remained close to their native configurations, thus allowing the SR Ca^{2+} release channels to retain their original gating properties.

$IpTx_a$-induced long-duration Ca^{2+} release events

The addition of 5–50 nM $IpTx_a$ to the internal solution bathing permeabilized frog skeletal muscle fibers resulted in the induction of discrete Ca^{2+} release events that were orders of magnitude longer than the spontaneously occurring Ca^{2+} sparks. The directly observed time courses of imperatoxin-induced events varied in duration from several hundred milliseconds to at least 1 s. The image acquisition was such that five successive 1-s images were obtained at a single location on the fiber, with a ~1-s separation between them, so no event longer then 1 s could be continuously observed. However, some events at a single triad extended through the entire duration of an image without a detectable beginning or termination of fluorescence, suggesting that there are events that have a time course considerably longer then 1 s. Using the frequency at which long events are initiated, together with the average total open time of all long events per 1-s image in the same images from the same fiber, the mean duration of the long events was determined to be 1.8 s in the series of experiments described in Fig. 4 and 2.6 s in the series of experiments in Fig. 2. These results agree closely with the results obtained for frog SR Ca^{2+} release channels exposed to $IpTx_a$ in planar lipid bilayer studies, where the mean open time of the subconductance state was 2.5 s (Fig. 6). Because $IpTx_a$ binds to the RyRs with high affinity, it appears that the prolonged presence of a toxin molecule at its binding site on the channel is directly responsible for the long duration of these events and that

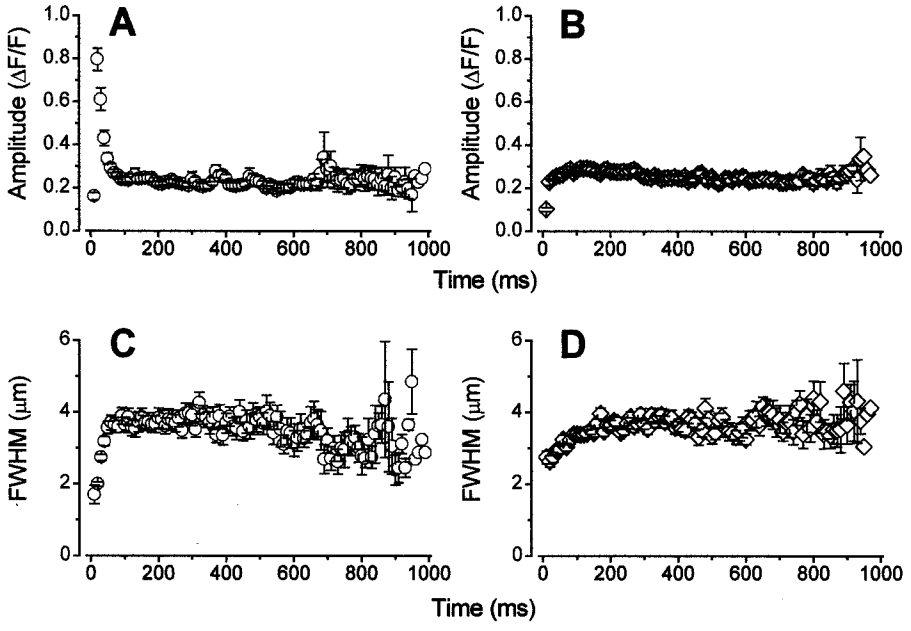

FIGURE 8 Average amplitudes of $\Delta F/F$ fluorescence determined at 10-ms intervals in the events that have a spark at the beginning of their time course (n_{events} = 62) (*A*) and the events that achieve a substate fluorescence immediately (n_{events} = 144) (*B*). (*C* and *D*) Average spatial half-widths determined at time intervals in events represented in *A* and *B*, respectively.

imperatoxin binding is capable of modulating a Ca^{2+} release channel in a way that would allow the attainment of a steady state between Ca^{2+} release and Ca^{2+} diffusion and binding to the contractile apparatus as well as other Ca^{2+} binding elements. It appears that $IpTx_a$ can directly activate only a single channel for a prolonged period of time. Any neighboring channels indirectly activated by Ca^{2+} released from the $IpTx_a$-activated channel should inactivate relatively rapidly and thus would not contribute to the observed long-duration events. Alternatively, if a single $IpTx_a$-activated channel could activate neighboring channels by direct molecular linkages (Marx et al., 1998), then the long-duration events could be due to the contribution of multiple channels. However, we have never observed such a coupled gating phenomenon in our bilayer studies. Multiple-channel insertion in bilayer, as reflected by "staircase" jumps in conductance, is frequently observed, but this is different from "coupled gating," where two or more channels gate coordinately to produce a single conductance. In the absence of such coupled gating, the observed long-duration events should reflect Ca^{2+} release from a single $IpTx_a$-activated channel.

Frog skeletal muscle has two RyR isoforms, α and β, which are homologous to the mammalian RyR1 and RyR3 isoforms, respectively (Sutko and Airey, 1996). These two isoforms could exhibit differences in response to $IpTx_a$. Possible differences in response might be due either to molecular differences in the isoforms or to differences in interaction of the isoforms with accessory proteins. In the present muscle fiber experiments we do not know whether $IpTx_a$ interacts with a single isoform or with either RyR isoforms to produce the long-duration Ca^{2+} release events. In bilayer experiments using frog SR, the activity of all detected channels was similar before and after exposure to $IpTx_a$ (Wang et al., 2000). Thus, either there are no differences in the isoforms, or only a single isoform is preferentially inserted into or active in the bilayer.

Imperatoxin-induced events have several distinct properties that separate them from the short Ca^{2+} sparks observed in the same muscle fibers. These properties include more than a 100-fold longer mean duration of imperatoxin-induced events compared to Ca^{2+} sparks, as well as an amplitude approximately one-third that of the sparks. The lower amplitudes of the long events compared to the spark are reminiscent of the subconductance states induced by the same peptide in the planar lipid bilayer experiments described by Tripathy et al. (1998) and Gurrola et al. (1999), as well as the present experiments carried out using Ca^{2+} release channels from frog SR vesicles (Figs. 3 and 6). However, the interpretation of this comparison requires consideration of the relationship between channel current and the resulting Ca^{2+} spark. The bilayer experiments provide a direct measurement of channel current, whereas the local fluorescence change in a muscle fiber is related to the integral of the Ca^{2+} efflux corrected for Ca^{2+} loss by diffusion and binding.

Based on the model described by Tripathy et al. (1998), $IpTx_a$ interacts with the Ca^{2+} release channel at a single, cytosolically accessible site while the channel is open. According to this model, the rate of $IpTx_a$ binding to the channel is linearly dependent on the concentration of imperatoxin, whereas the rate of $IpTx_a$ dissociation from the subconductance state is independent of it. We have tested this model in skeletal muscle fibers, using 10, 25, and 50 nM $IpTx_a$, and found that the frequency of occurrence of imperatoxin-induced, long-duration events was directly proportional to the concentration of $IpTx_a$ (Fig. 4 *A*). Although the tested [$IpTx_a$] was far from saturating levels, the appearance of the first-order response to the imperatoxin concentrations leads us to believe that a single molecule of $IpTx_a$ interacts with a single Ca^{2+} release channel during the induction of long-duration Ca^{2+} release events. However, binding studies (Gurrola et al., 1999) and cryoelectron microscopy (Samso et al., 1999) indicate a binding stoichiometry of four $IpTx_a$ molecules per Ca^{2+} release channel. Thus the present data indicate that binding of $IpTx_a$ to one of four possible sites may be sufficient to activate the channel. Because the mean open time of $IpTx_a$-induced events is independent of [$IpTx_a$], possible binding of more than one toxin molecule does not appear to alter the control of channel conductance by the first toxin molecule. Perhaps only one of the four possible binding sites is capable of producing a functional response due to the binding of $IpTx_a$.

We also determined that the total open time of the substates also exhibited a dose-dependent response (Fig. 4 *B*). However, the mean open time of each event remained relatively constant at all tested $IpTx_a$ concentrations (Fig. 4 *C*). According to these results, the mean open time of a channel in the substate is independent of the ligand concentration, as originally suggested by Tripathy et al. (1998). This provides further evidence that frequency of occurrence of imperatoxin-induced events in muscle fibers is dependent on the rate at which $IpTx_a$ binds to the channel and not on the rate of its dissociation.

In our experiments most of the imperatoxin-induced events were detected as a change in fluorescence, either at the beginning or at the end of their time course. Analysis of the fluorescence at the beginning of the time course has shown that 38% of the events in experiments described in Fig. 2 and 30% of the events described in Fig. 4 had a spark-like beginning, whereas the rest of the events did not. As shown in Fig. 8, the fluorescence time courses of these events were significantly different. Events that did not begin with a spark achieved steady state fluorescence very rapidly, ~20 ms after the initiation, whereas the events that begin with a spark jumped up rapidly, then declined and finally attained the steady state ~45–50 ms after their initiation. This observation can be interpreted in several ways. As reported by Tripathy et al. (1998), there is a strong indica-

tion that $IpTx_a$ modulates Ca^{2+} release by interacting with open channels. If this is the case, imperatoxin might be involved in the termination of the initial spark. This termination might occur at various phases of Ca^{2+} release from the channel. If $IpTx_a$ interacts with the channel during the early phase of Ca^{2+} release, it could be involved in the termination of the spark before the attainment of maximum amplitude. If this were to occur relatively early during the rising phase of the spark, the long event would not appear to have a spark at the beginning of its time course. On the other hand, if imperatoxin interacts with the channel near the time that peak amplitude would be achieved, the substate will appear to have a spark at the beginning of its time course. As an alternative possibility, the two types of induction of long events might also arise from the fact that imperatoxin may interact with channels that are either open or closed. This interpretation, however, requires that $IpTx_a$ is capable of modulating a closed channel.

The probability of a large number of independent events occurring at the same active triad is extremely low (Klein et al., 1999), suggesting that an imperatoxin-induced event does not arise from openings of multiple independent SR release units at the same triad. The activity of the channels during $IpTx_a$-induced activation may correspond to an SR channel being constantly held open or having a very rapid rate of reopening. In either case, the differences in amplitudes between the spark at the beginning and the plateau interval of the long-duration fluorescence time course cannot arise from the differences in relative position of the origin of Ca^{2+} release relative to the location of the confocal linescan (Pratusevich and Balke, 1996), because these two events can be assumed to arise from the same spatial location. Initiation of both the spark and the subsequent long-duration event at the same focal origin provides the means of compensating for the inability to determine where the events occur relative to the location of the confocal linescan. This allows for the accurate determination of the spatiotemporal properties of the long-duration events in relation to Ca^{2+} sparks, regardless of the fact that the events may not be completely in focus.

$IpTx_a$ events and the number of Ca^{2+} release channels active during a short-duration Ca^{2+} spark

Based on the preceding considerations, it seems likely that the long-duration events observed in permeabilized frog muscle fibers in the presence of $IpTx_a$ are generated by the opening of a single SR Ca^{2+} release channel to a subconductance state. If this interpretation is correct, then the steady-state fluorescence level during the long events provides a reference "benchmark" for the local fluorescence that can be generated by the steady opening of a single SR channel to the subconductance state. This benchmark can then be used to attempt to estimate the number of channels that may be involved in generating a normal, short-duration Ca^{2+} spark.

Let us assume that the ratio of currents through a channel in the sub- and full-conductance states in the fibers is the same as the mean value of 28% determined for frog channels in the present bilayer experiments. Because model simulations indicate that the local fluorescence change produced by a point current source at the triad is directly proportional to the current amplitude (Jiang et al., 1999), the steady opening of a single channel to the full-conductance state in the fiber would thus be expected to produce a local fluorescence change ~3.6 times larger (i.e., 1/0.28) than the fluorescence during the long toxin-induced events. The mean value of the ratio of steady fluorescence to peak fluorescence in long events with a spark at the start was 31%, so the mean value of the peak fluorescence change during sparks at the start of long $IpTx_a$-induced events was 3.2 times larger then the steady fluorescence during the long events. Thus the peak fluorescence change in the spark was fortuitously approximately equal (i.e., 3.2/3.6 or 89%) to the fluorescence change that would have been produced by the prolonged opening of a single SR channel to the full conductance state in the fiber. However, the duration of channel activity during a spark is too brief to attain the steady fluorescence that would be produced by prolonged opening of the channels active in a spark. Thus, to use the preceding information to estimate the number of channels generating the spark, we must estimate the steady fluorescence change that would have been attained if the channels that open briefly during the spark had remained open long enough to attain steady fluorescence. For example, if the steady fluorescence produced by prolonged opening of the spark channels were estimated to be twice the peak fluorescence change in the spark, we would conclude that the spark was generated by the opening of two SR Ca^{2+} release channels to the full conductance state.

We have two means of estimating the increase in fluorescence change that would have occurred had the spark channels remained open for a prolonged period of time. First, model simulations (Jiang et al., 1999) indicate that an 8-ms constant current from a point source at the triad gives rise to a simulated Ca^{2+} spark that has a rise time (10–90%) close to the mean spark rise time determined with the confocal system used in the present muscle fiber experiments. Simulations with the same model parameter values but with a prolonged current show that the steady fluorescence change that is attained is ~1.17 times larger than the peak of the spark simulated for 8 ms of the same current (L. Zhu, Y. H. Jiang, and M. F. Schneider, unpublished result; Zhu et al., 1999b). Thus these simulations and the above reasoning suggest that a spark might be generated by the activity of a single SR Ca^{2+} release channel.

As an alternative approach, fits to the time course of the rising phase of sparks recorded with a high time resolution (63 μs/line) confocal system demonstrate that the rising

phase of a spark is well described by the expression $A\{1 - \exp[k_1(t - d_1)]\}$, where A is the amplitude the fluorescence change would be expected to attain during continuous opening of the channels, k_1 is the rate constant for the rising phase of the spark, t is time, and d_1 is the time of the start of the spark (Lacampagne et al., 1999). Using this theoretical expression for the time course of the rising phase of the spark, the ratio of the steady fluorescence change for prolonged opening of the spark channel(s) to the peak spark fluorescence is given by $\{1 - \exp[k_1(d_2 - d_1)]\}^{-1}$, where d_2 is the time of the peak of the spark (i.e., $d_2 - d_1$ is the duration of the rising phase of the spark). From the results of the fits to 198 high time resolution sparks reported by Lacampagne et al. (1999), the mean value of this expression is 1.40 ± 0.06 (mean ± SEM; A. Lacampagne, M.G. Klein, C.W. Ward, and M.F. Schneider, unpublished results). The peak amplitude of the sparks recorded with the present lower time resolution (2 ms/line) confocal system may have been underestimated somewhat by temporal undersampling. In this case the ratio of expected fluorescence for steady opening of the spark channels to the recorded peak amplitude of the spark would be somewhat larger, perhaps closer to 2, and thus consistent with two channels being involved in generating a spark. Thus both lines of reasoning indicate that the number of channels involved in a spark was relatively small, perhaps one or two channels open to the full-conductance state. These values come from predictions of steady fluorescence from peak spark fluorescence, using either model simulations or the extrapolation of observed time courses of the rising phases of measured sparks to times after the peak of the spark, and thus involve some uncertainty. Using sparks of relatively large amplitude, tests of the smoothing (3 × 3 boxcar) and spatial averaging methods used to obtain the records from which peak spark fluorescence was determined indicate that the true value of spark peak amplitude, and thus the expected steady fluorescence change, might be ~25% larger than the values obtained with the spark analysis procedures used here. However, it seems unlikely that the true value of the fluorescence change attained during steady opening of the spark channels would be more than about twice the values estimated here, in which case the number of channels involved in generating a spark would be at most four, and possibly fewer. The larger recent estimates of the number of channels contributing to a spark is based on a larger observed value of peak amplitude of the "starter" spark relative to the steady fluorescence of the subsequent $IpTx_a$-induced events (Gonzalez et al., 2000).

Our estimate of the number of channels in a spark is based on the assumption that each $IpTx_a$-induced long event is generated by the subconductance opening of a single $IpTx_a$-bound channel. If more then one channel were involved in the long event, then our estimate of the number of channels in a spark would have to be increased proportionally. However, this seems unlikely because our observations of linear concentration dependence of long event frequency and the similarity of mean event duration in fibers and mean open time of $IpTx_a$-induced subconductance channel opening in bilayers argue against multiple $IpTx_a$-bound channels being involved in a long event. Furthermore, any neighboring toxin-free channels opened by CICR from a toxin-bound channel would rapidly inactivate and should thus be unavailable to contribute to a long event. Finally, if multiple neighboring channels were directly coupled to a single $IpTx_a$-activated channel (Marx et al., 1998), those coupled channels would be expected to open to the full conductance rather than to a subconductance state. In this case, the long events would have similar or even larger amplitude than a Ca^{2+} spark, which is contrary to our observations.

In conclusion, imperatoxin A induces long-duration Ca^{2+} release events in frog permeabilized skeletal muscle fibers. These long-duration events are analogous to the long-duration subconductance states induced by the same toxin in frog single SR Ca^{2+} release channels reconstituted in planar lipid bilayer. It thus appears that $IpTx_a$ produces long-duration Ca^{2+} release events in muscle fibers by directly activating a single Ca^{2+} release channel to a subconductance state for a prolonged period of time.

We thank Dr. Peace Cheng for supplying the source code for the automatic spark detection routine (Cheng et al., 1999).

This work was supported by research grants and fellowships from the National Institutes of Health (R01-NS23346 to MFS, AR08544-02 to CWW, and PO1 HL47053 to HHV). HHV is a recipient of an Established Investigator Award from the American Heart Association.

REFERENCES

Cheng, H., W. J. Lederer, and M. B. Cannell. 1993. Calcium sparks: elementary events underlying excitation-contraction coupling in heart muscle. *Science.* 262:740–744.

Cheng, H., L. S. Song, N. Shirokova, A. Gonzalez, E. G. Lakatta, E. Rios, and M. D. Stern. 1999. Amplitude distribution of calcium sparks in confocal images: theory and studies with an automatic detection method. *Biophys. J.* 76:606–617.

Colquhoun, D., and A. G. Hawkes. 1983. The principles of the stochastic interpretation of ion-channel mechanisms. In Single-Channel Recording. B. Sakmann and E. Neher, editors. Plenum Press, New York. 135–175.

El-Hayek, R., B. Antoniu, J. Wang, S. L. Hamilton, and N. Ikemoto. 1995. Identification of calcium release-triggering and blocking of the II-III loop of the skeletal muscle dihydropyridine receptor. *J. Biol. Chem.* 270:22116–22118.

Franzini-Armstrong, C., F. Protasi, and V. Ramesh. 1999. Shape, size, and distribution of Ca^{2+} release units and couplons in skeletal and cardiac muscles. *Biophys. J.* 77:1528–1539.

Gonzalez, A., W. G. Kirsch, N. Shirokova, G. Rizarro, G. Brum, I. N. Pessah, M. D. Stern, H. Cheng, and E. Rios. 2000. Involvement of multiple intracellular release channels in calcium sparks of skeletal muscle. *Proc. Natl. Acad. Sci. USA*. 97:4380–4385.

Gurrola, G. B., C. Arevalo, R. Sreekumar, A. J. Lokuta, J. W. Walker, and H. H. Valdivia. 1999. Activation or ryanodine receptors by imperatoxin A and a peptide segment of the II-III loop of the dihydropyridine receptor. *J. Biol. Chem.* 274:7879–7886.

Jiang, Y. H., M. G. Klein, and M. F. Schneider. 1999. Numerical simulation of Ca^{2+} "Sparks" in skeletal muscle. *Biophys. J.* 77:2333–2357.

Klein, M. G., H. Cheng, L. F. Santana, Y.-H. Jiang, W. J. Lederer, and M. F. Schneider. 1996. Two mechanisms of quantized calcium release in skeletal muscle. *Nature.* 379:455–458.

Klein, M. G., A. Lacampagne, and M. F. Schneider. 1997. Voltage dependence of the pattern and frequency of discrete Ca^{2+} release events after brief repriming in frog skeletal muscle. *Proc. Natl. Acad. Sci. USA.* 94:11061–11066.

Klein, M. G., A. Lacampagne, and M. F. Schneider. 1999. A repetitive mode of activation of discrete Ca^{2+} release events (Ca^{2+} sparks) in frog skeletal muscle fibers. *J. Physiol. (Lond.).* 515:391–411.

Lacampagne, A., M. G. Klein, and M. F. Schneider. 1998. Modulation of the Frequency of spontaneous sarcoplasmic reticulum Ca^{2+} release events (Ca^{2+} sparks) by myoplasmic [Mg^{2+}] in frog skeletal muscle. *J. Gen. Physiol.* 111:207–224.

Lacampagne, A., W. J. Lederer, M. F. Schneider, and M. G. Klein. 1996. Repriming and activation alter the frequency of stereotyped discrete Ca^{2+} release events in frog skeletal muscle. *J. Physiol. (Lond.).* 497: 581–588.

Lacampagne, A., C. W. Ward, M. G. Klein, and M. F. Schneider. 1999. Time course of individual Ca^{2+} sparks in frog skeletal muscle recorded at high time resolution. *J. Gen. Physiol.* 113:187–198.

Leong, P., and D. H. MacLennan. 1998. A 37-amino acid sequence in the skeletal muscle ryanodine receptor interacts with the cytoplasmic loop between domains II-III in the skeletal muscle dihydropyridine receptor. *J. Biol. Chem.* 273:7791–7794.

Marx, S. O., K. Ondrias, and A. R. Marks. 1998. Coupled gating between individual skeletal muscle Ca^{2+} release channels (ryanodine receptors). *Science.* 281:818–821.

Meltzer, W., A. Herrmann-Frank, and H. Ch. Lüttgau. 1995. The role of Ca^{2+} ions in excitation-contraction coupling of skeletal muscle fibres. *Biochim. Biophys. Acta.* 1241:59–116.

Nakai, J., T. Tanabe, T. Konno, B. Adams, and K. G. Beam. 1998. Localization in the II-III loop of the dihydropyridine receptor of a sequence critical for excitation-contraction coupling. *J. Biol. Chem.* 273:24983–24986.

Pratusevich, V. R., and C. W. Balke. 1996. Factors shaping confocal image of the calcium spark in cardiac muscle cells. *Biophys. J.* 71:2942–2957.

Rios, E., M. D. Stern, A. Gonzalez, G. Pizarro, and N. Shirokova. 1999. Calcium release flux underlying Ca^{2+} sparks of frog skeletal muscle. *J. Gen. Physiol.* 114:31–48.

Samso, R., Trujillo, G. B. Gurrola, H. H. Valdivia, and T. Wagenknecht. 1999. Three-dimensional location of the Imperatoxin A binding site on the ryanodine receptor. *J. Cell. Biol.* 146:493–499.

Schneider, M. F. 1994. Control of calcium release in functioning skeletal muscle fibers. *Annu. Rev. Physiol.* 56:463–484.

Schneider, M. F. 1999. Ca^{2+} sparks in frog skeletal muscle: generation by one, some, or many SR Ca^{2+} release channels. *J. Gen. Physiol.* 113: 365–371.

Schneider, M. F., and M. G. Klein. 1996. Sarcoplasmic calcium sparks activated by fiber depolarization and by cytosolic Ca^{2+} in skeletal muscle. *Cell Calcium.* 20:123–128.

Shtifman, A., C. W. Ward, H. H. Valdivia, and M. F. Schneider. 1999. Induction of long duration Ca^{2+} release events by imperatoxin A in frog skeletal muscle. *Biophys. J.* 76:A465.

Sutko, J. L., and J. A. Airey. 1996. Ryanodine receptor Ca^{2+} release channels: Does diversity in form equal diversity in function? *Physiol. Rev.* 76:1027–1071.

Tanabe, T., K. G. Beam, B. A. Adams, T. Niidome, and S. Numa. 1990. Regions of the skeletal muscle dihydropyridine receptor critical for excitation-contraction coupling. *Nature.* 346:567–569.

Tripathy, A., W. Resch, L. Xu, H. H. Valdivia, and G. Meissner. 1998. Imperatoxin A induces subconductance states in Ca^{2+} release channels (ryanodine receptors) of cardiac and skeletal muscle. *J. Gen. Physiol.* 111:679–690.

Tsuchiya, T. 1988. Passive interaction between sliding filaments in the osmotically compressed skinned muscle fibers of the frog. *Biophys. J.* 53:415–423.

Tsugorka, A., E. Rios, and L. A. Blatter. 1995. Imaging elementary events of calcium release in skeletal muscle cells. *Science.* 269:1723–1726.

Valdivia, H. H., J. H. Kaplan, G. C. Ellis-Davies, and W. J. Lederer. 1995. Rapid adaptation of cardiac ryanodine receptors: modulation by Mg^{2+} and phosphorylation. *Science.* 267:1997–2000.

Wang, J., O. Fuentes, X. Zhu, and H. H. Valdivia. 2000. α and β ryanodine receptor isoforms of frog skeletal muscle display no obvious functional difference in their response to Ca^{2+} and imperatoxin A. *Biophys. J.* 78:425A.

Ward, C. W., A. Lacampagne, M. G. Klein, and M. F. Schneider. 1998. Ca^{2+} spark properties in saponin permeabilized skeletal muscle. *Biophys. J.* 72:A269.

Zamudio, F. Z., G. B. Gurrola, C. Arevalo, R. Sreekumar, J. W. Walker, H. H. Valdivia, and L. D. Possani. 1997. Primary structure and synthesis of imperatoxin A ($IpTx_a$), a peptide activator of Ca^{2+} release channels/ ryanodine receptors. *FEBS Lett.* 405:385–389.

Zhu, X., G. B. Gurrola, M. T. Jiang, J. W. Walker, and H. H. Valdivia. 1999a. Conversion of an active cardiac dihydropyridine receptor II-III loop segment into forms that activate skeletal ryanodine receptors. *FEBS Lett.* 450:221–226.

Zhu, L., Y.-H. Jiang, C. W. Ward, A. Shtifman, H. H. Valdivia, and M. F. Schneider. 1999b. Numerical simulation of long duration calcium release events induced by $IpTx_a$. *Biophys. J.* 76:A464.